Journal of
Materials Chemistry C

Materials for optical, magnetic and electronic devices

Accepted Manuscript

This article can be cited before page numbers have been issued, to do this please use: M. Jeong, D. K. Moon, H. S. Kim and J. H. Kim, *J. Mater. Chem. C*, 2020, DOI: 10.1039/D0TC02513E.

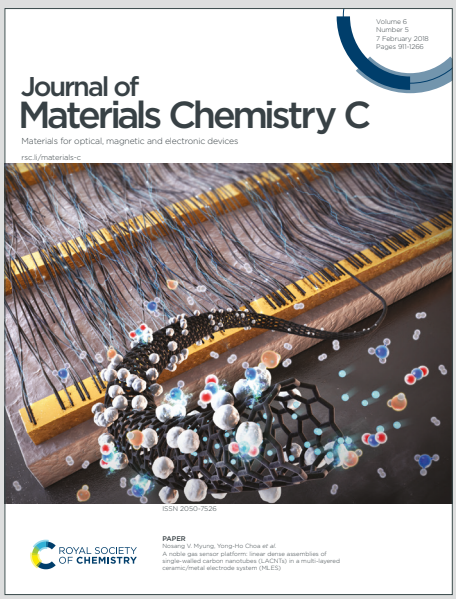

ROYAL SOCIETY OF CHEMISTRY

rsc.li/materials-c

View Article Online
DOI: 10.1039/D0TC02513E

ARTICLE

Small-molecule electrolytes with different ionic functionality as cathode buffer layer for polymer solar cells

Received 00th January 20xx,
Accepted 00th January 20xx

DOI: 10.1039/x0xx00000x

Mijin Jeong[a], Doo Kyung Moon[b], Hyun Sung Kim[*,c], Joo Hyun Kim[*,a]

In polymer solar cells (PSCs), electrolytes as the cathode interlayer are responsible for generating an interface dipole, which reduces the charge collection barrier at the cathode interface. In this study, small-molecule electrolytes were designed and synthesized as the cathode interlayer in inverted PSCs to overcome high processing costs caused by complicated synthesis procedures. Moreover, the proposed design strategy allows the ion size and number of ionic functionalities to tune the magnitude of the interface dipole. The structures of ((benzene-1,2,4,5-tetrayltetrakis(methylene))tetrakis(triphenylphosphonium) bromide) (**4PBr**) comprises a phenyl core with four benzyl triphenylphosphonium salts and (N,N'-(1,2-phenylenebis(methylene))bis(N,N-diethylethanaminium) bromide) (**2EBr**) has two benzyl trialkyl ammonium salts. The device based on **4PBr** exhibited a power conversion efficiency of 10.63% (J_{sc} = 20.2 mA/cm^2, V_{oc} = 0.79 V, *FF* = 66.6%), which is superior to that with **2EBr** (PCE = 9.56%, J_{sc} = 19.7 mA/cm^2, V_{oc} = 0.80 V, *FF* = 61.1%). Thus, we demonstrated the possibility of maximizing performances without complicated synthesis procedures.

Introduction

Over the last decade, there have been several approaches in developing highly efficient polymer solar cells (PSCs) due its processability, flexibility, and low-cost fabrication in large-area applications.[1–4] Outstanding improvements with power conversion efficiencies (PCE) of up to 16%[5] have been achieved by developing efficient photoactive materials[6–16] and interface engineering the electrode.[17–37] Among these, tuning the energy offset at the cathode interface is an important issue that should be addressed to enhance electron collection ability.

ZnO has been commonly used as the electron transport layer in inverted PSCs. To maximize its electron collection ability, there have been several approaches in changing its layer properties, such as inserting conjugated/non-conjugated polymer electrolytes[17–30] as the interlayer and self-assembled monolayer[31–34] treatments. Thus, better PCEs was achieved by reducing the energy offset at the cathode interface and enhancing the charge collection capability.

Conjugated polymer electrolytes (CPEs) have been widely used as the cathode interlayer. However, CPEs have complicated synthetic procedures and extremely low product yield, limiting their commercial large-area application. In terms of processing cost, the development of small-molecule organic electrolytes[38–45] with simple synthetic procedures can attract attention in large-area application. Recently, we reported the effect of the size of the counter anion[36] and cation[46] of organic electrolytes on the photovoltaic properties. The results suggested that a lager counter ion leads to a larger interface dipole, indicating its influence on the energy offset at the cathode interface. Lee et al. and Jo et al. also reported that the number of ionic functionalities on electrolytes affect the performance of PSCs.[47–49] This suggests that the magnitude interface dipole depends on the number of ionic functionalities. Moreover, the size of ions and number of ionic functionalities have been observed to efficiently reduce the charge collection barrier at the interface, thereby improving device performances.

With hese, we designed and synthesized (N,N'-(1,2-phenylenebis (methylene))bis(N,N-diethylethanaminium) bromide) (**2EBr**) and ((benzene-1,2,4,5-tetrayltetrakis (methylene))tetrakis (triphenylphosphonium) bromide) (**4PBr**) (shown in **Figure 1a**). Both **2EBr** and **4PBr** have the advantage of allowing mass production without a complex synthetic procedure and low product yield. The dipole moment of the ionic compound is proportional to the distance between two charges. Therefore, the dipole moment of triphenyl phosphonium salt would be larger than that of triethyl ammonium salt. In addition to this, **4PBr** is expected to have a higher dipole moment than **2EBr** due to the number of ionic functionalities. The device based on a bulk-heterojunction structure (**Figure 1b**) composed of poly([2,6'-4,8-di(5-ethylhexylthienyl)benzo[1,2-b;3,3-b]dithiophene]{3-fluoro-2[(2-ethylhexyl)carbonyl]thieno[3,4-b]thiophenediyl}) (PTB7-Th) and [6,6]-phenyl C71 butyric acid methyl ester ($PC_{71}BM$) (**Figure 1c**) as the active layer enhances the PCE based on ZnO from 8.75% (short circuit current J_{sc} = 17.5 mA/cm^2, open circuit voltage V_{oc} = 0.80 V, fill factor *FF* = 62.5%) to 10.63% (J_{sc} = 20.2 mA/cm^2, V_{oc} = 0.79 V, *FF* = 66.6%), by introducing **4PBr** as the interlayer. Moreover, the device based on **4PBr** hasa more

[a] Department of Polymer Engineering, Pukyong National University, Busan 48513, Korea
[b] Division of Chemical Engineering, Konkuk University, Seoul 05029, Korea
[c] Department of Chemistry, Pukyong National University, Busan 48513, Korea
Electronic Supplementary Information (ESI) available: Experimental details including materials, synthesis, measurements, and fabrication of devices
* corresponding Authors. Kimhs75@pknu.ac.kr, jkim@pknu.ac.kr

View Article Online
DOI: 10.1039/D0TC02513E

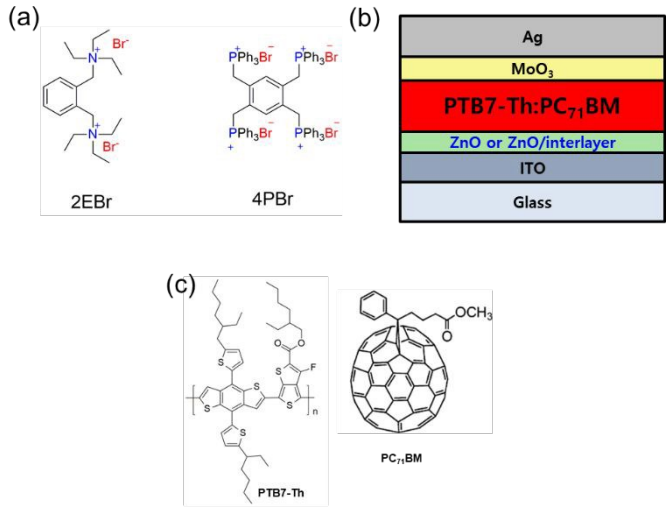

Figure 1. Chemical structure of (a) small-molecule electrolytes and (b) PTB7-Th and $PC_{71}BM$. (c) Device structure of PSC used in this study.

superior PCE than that based on **2EBr** (PCE = 9.56%, J_{sc} = 19.7 mA/cm², V_{oc} = 0.80 V, *FF* = 61.1%). This could be mainly attributed to the improved J_{sc} by the reduced Schottky barrier at the cathode interface.

Results and Discussion

2EBr and **4PBr** were synthesized by simple substitution reaction between 1,2-bis(bromomethyl)benzene and triethylamine in toluene and acetonitril, respectively. All compounds were well characterized by the ^{1}H, ^{13}C NMR, and elemental analysis, which are provided in the Supplementary Information.

We fabricated the inverted type PSCs (illustrated in **Figure 1b**) based on ZnO with and without small-molecule electrolytes as the electron transporting layer and investigated the effect of ionic functionality on the photovoltaic properties. Detailed procedures for the fabrication of PSCs are described in the Supplementary Information and the photovoltaic parameters with different thickness of the cathode interlayer are summarized in **Table S1**. The optimum thickness of the interlayer was determined to be 5□6 nm. As shown in Figure S1, small-molecule electrolytes do not tend to aggregate on the surface of ZnO. The surface roughness of the ZnO surface with 2EBr and 4PBr were 0.58 and 0.60 nm, respectively, which are comparable to the surface roughness of ZnO surface (0.55 nm). **Figure 2a** shows the current density–voltage (*J–V*) curves of PSCs with and without interlayer under illumination while the photovoltaic performances are summarized in **Table 1**. Significant enhancements are observed in devices based on ZnO with an interlayer. The PCEs of devices with **2EBr** and **4PBr** are 9.56% (J_{sc} =19.7 mA/cm², V_{oc} = 0.80 V, FF = 61.1%) and 10.63% (J_{sc} = 20.2 mA/cm², V_{oc} = 0.79 V, *FF* = 66.6%), while that based on ZnO without interlayer was limited to 8.75% (J_{sc} =17.5 mA/cm², V_{oc} = 0.80 V, *FF* = 62.5%). Noticeably, the enhanced J_{sc} was the main contributor of the improved PCE.

Kelvin probe microscopy (KPM) is a common powerful tool for determining the effective work function of a metal or metal oxide. Thus, KPM measurements were conducted to investigate how the interlayer affects the changes of J_{sc}.[21–23,26,27,36,37,42-46,48] A larger Schottky barrier at the interface interrupts charge collection capability.

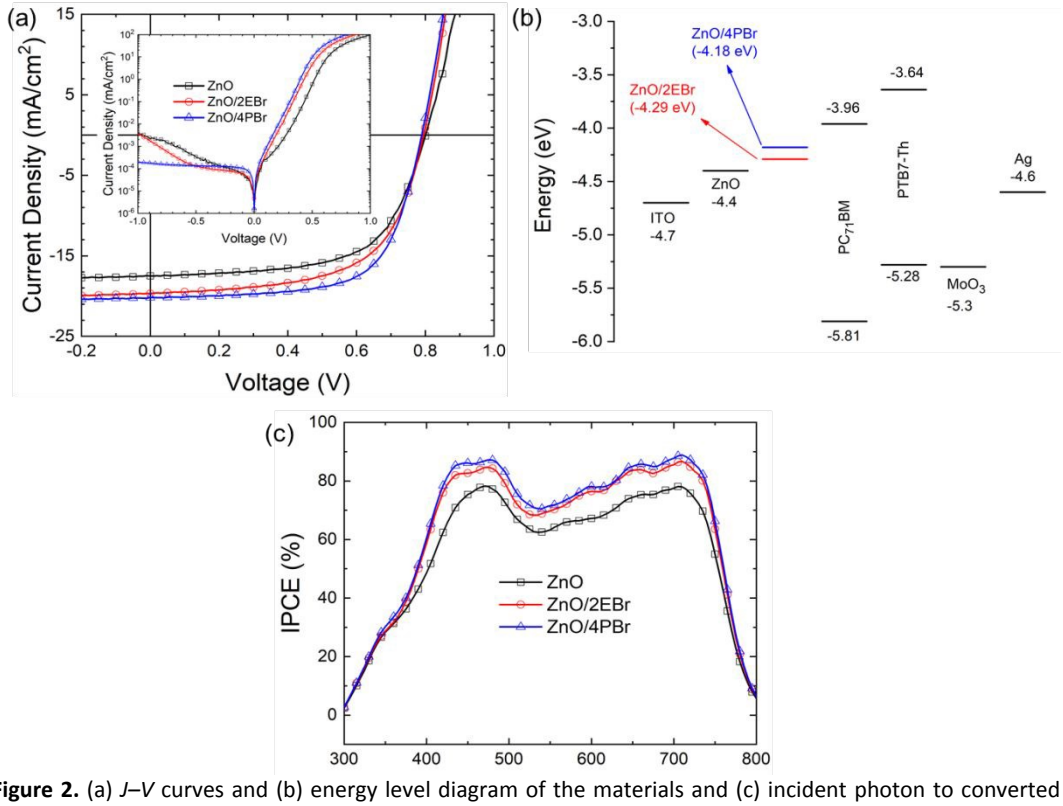

Figure 2. (a) *J–V* curves and (b) energy level diagram of the materials and (c) incident photon to converted electron (IPCE) curves of the PSCs at the optimum processing condition.

View Article Online
DOI: 10.1039/D0TC02513E

Table 1. Photovoltaic parameters of PSCs based on ZnO/interlayer. The averages (10 devices) are shown in parentheses.

Interlayer	J_{sc} (mA/cm²)	V_{oc} (V)	FF (%)	PCE (%)	$J_{sc,cal}$[a] (mA/cm²)	R_s[b] (Ω·cm²)	R_{sh}[c] (kΩ·cm²)
-	17.5 (17.3)	0.80 (0.80)	62.5 (62.7)	8.75 (8.69)	17.1	3.29	893
2EBr	19.7 (19.6)	0.80 (0.80)	61.1 (60.4)	9.56 (9.41)	19.1	2.60	645
4PBr	20.2 (20.1)	0.79 (0.79)	66.6 (65.2)	10.63 (10.29)	19.6	2.28	2533

[a] Calculated from IPCE curves. [b,c]Series and shunt resistance data are calculated from the device showing the best PCE.

Thus, the transition from a Schottky to Ohmic contact at the interface is a crucial factor to achieve high J_{sc}. As shown in **Figure 2b**, the work function of ZnO with **2EBr** and **4PBr** is −4.29 and −4.18 eV, respectively, while that of ZnO was −4.4 eV. The change in magnitude of the interface dipole depended on changing the size of the cation and number of ionic functionalities. Reducing the Schottky barrier height results to a high J_{sc}, which is strongly related to the change of work function. Herein, the improved J_{sc} indicates the formation of favorable interface dipole with its magnitude depending on the ion size and number of ionic functionalities. The calculated J_{sc} data from IPCE curves (**Figure 2c**) showed an extremely good correlation with the J_{sc} data of devices under a simulated illumination of 1.0 sun. The series resistance (R_s) and shunt resistance (R_{sh}) were calculated from the inverse slope near the high current regime and the slope near the lower current region in the dark J–V curves. The R_s data also showed its coherence with the J_{sc} of PSCs. The R_{sh} data of the device based on pure ZnO, and ZnO with 2EBr, and 4PBr were 893, 645, and 2553 kΩcm², respectively, which are well correlated with their FF. Interestingly, the $R_{sh}$of the device based on 2EBr was smaller than that without interlayer.

To elucidate the effect of the interlayer on the electron transporting/collecting property of ZnO, we fabricated and tested the electron devices with a structure of ITO/ZnO (25 nm)/with or without interlayer (60 nm)/$PC_{71}BM$/Al (100 nm) (**Figure 3**). **Figure 3** shows the space-charge limited current (SCLC) characteristic of the current density and voltage. The electron mobilities of the devices were calculated by the SCLC method expressed by the Mott-Gurney Law. The electron mobilities of the devices based on **2EBr** and **4PBr** were 9.2×10^{-4} and 1.2×10^{-3} cm²/Vs, respectively, which are comparable to the device based on ZnO without interlayer (7.4×10^{-3} cm²/Vs). However, the turn-on voltages of the devices with **2EBr** and **4PBr**, which was estimated according to Parker,[49] were 1.26 and 0.94 V, respectively, while that based on ZnO without interlayer was limited to 1.65 V. Thus, the interlayer facilitates the electron collection capability from $PC_{71}BM$ layer to ZnO layer, owing to the introduced interlayer that reduced the Schottky barrier between them. Moreover, **4PBr** has easier electron collection ability than **2EBr**. These results are well coherent with the improvement of J_{sc}.

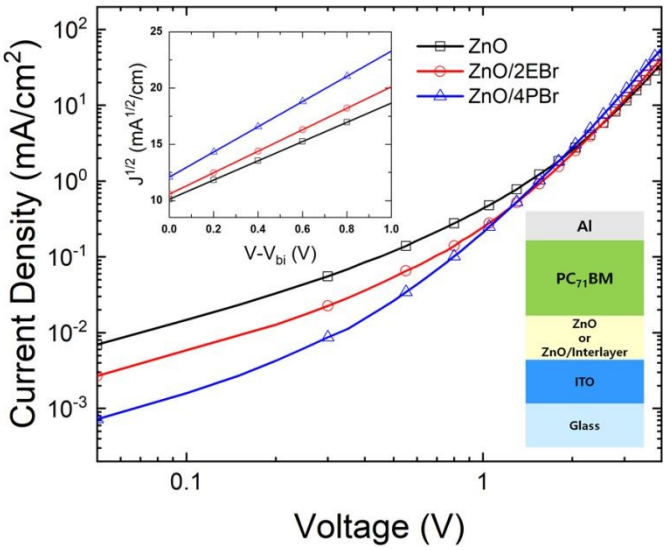

Figure 3. Current density–voltage curves of electron-only device with a configuration of ITO/ZnO (25 nm)/interlayer/$PC_{71}BM$ (60 nm)/Al (100 nm). (inset: with fitted line,V: applied voltage, V_{bi}: built-in voltage.

To understand the charge transport and collection properties of the devices, we analyzed the photocurrent density (J_{ph}) as a function of the effective voltage (V_{eff}) by:

$J_{ph} = J_L - J_D$

$V_{eff} = V_0 - V_a$

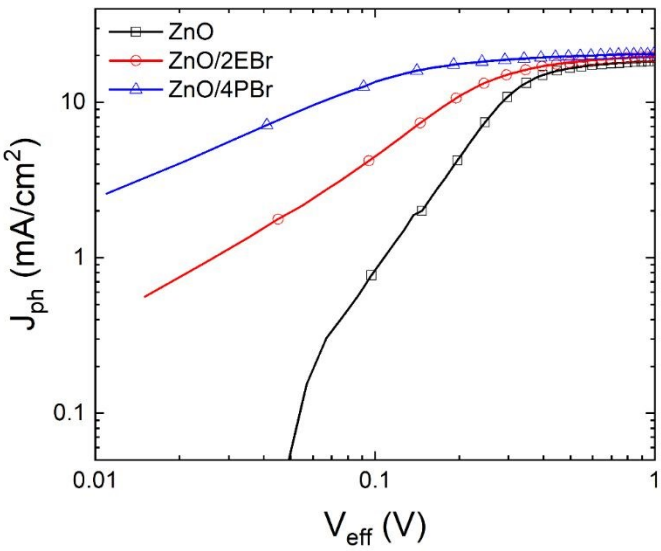

Figure 4. J_{ph} as a function of V_{eff} curves the PSCs.

where J_L is the measured current density under illumination, J_D is the measured current density without illumination, V_0 is the voltage at J_{ph}=0, and V_a is the applied voltage.

As shown in **Figure 4**, the log (J_{ph}) as a function of log (V_{eff}) showed a linear relationship at low V_{eff} and saturated at the high V_{eff} regime. The V_{eff} value of the devices reaching the saturated photocurrent (V_{sat}) increased in the following order: **4PBr** (0.17 V) < **2EBr** (0.31 V) ≅ ZnO (0.34 V). Hence, a smaller V_{sat} denotes faster transition from the space-charge-limited to the saturation regime. The results followed the trend of the J_{sc} and PCE of the devices.

We examined the J_{sc} and V_{oc} of the devices as a function of illumination intensity[50–52] to understand the charge recombination kinetics at the interfaces. The relationship between J_{sc} and illumination intensity I is generally defined by $J_{sc} \propto I^{\alpha}$. When the device exhibits a completely bimolecular recombination under short-circuit condition, α is unity. As shown in **Figure 5a**, the α of the devices based on ZnO with **2EBr** and **4PBr** are both 0.97, which is comparable to that based on ZnO (0.93). This indicates that the devices exhibited the suppression of undesirable bimolecular recombination. V_{oc} is defined by

$$V_{oc} \propto skT/q \cdot ln\,(I)$$

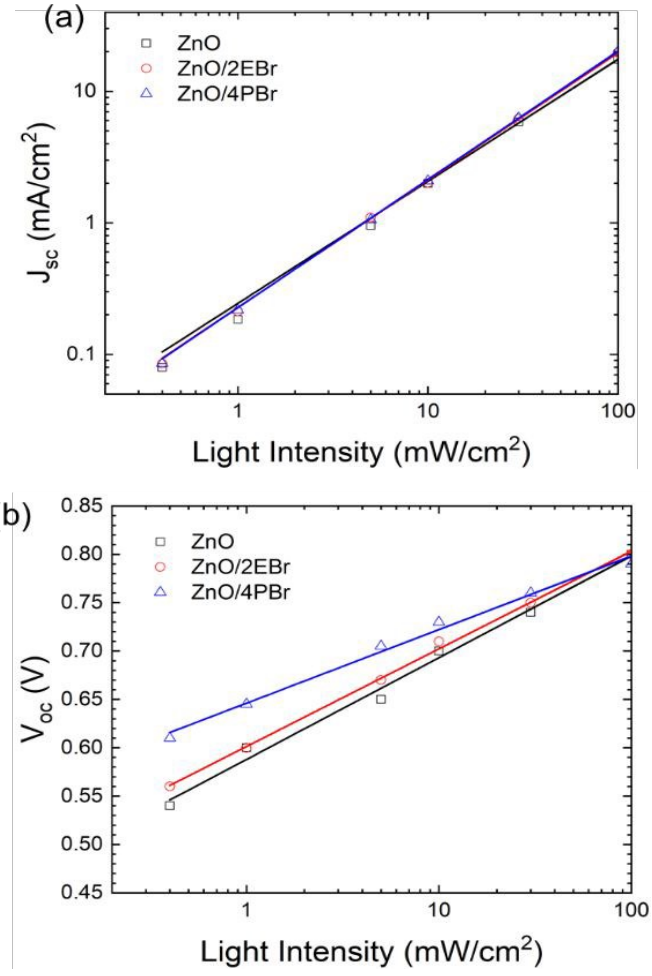

Figure 5. (a) J_{sc} – light intensity and (b) V_{oc} – light intensity plots of the PSCs.

where k, T, q, and I are the Boltzmann constant, temperature in Kelvin, electron charge, and illumination intensity, respectively. When bimolecular recombination is dominated, s is approximately equal to 1 and reaches 2 in the case of dominant trap-assisted recombination. The s values of the device based on pure ZnO, with **2EBr,** and with **4PBr** were 1.78, 1.71, and 1.29, respectively. Therefore, the lowest trap-assisted recombination behavior of the device based on **4PBr** can justify its highest J_{sc} and *FF* values. Overall, most device parameters related to the charge extraction and recombination characteristics of the devices are continuously improved by introducing the interlayer. In addition, the change in the s values of the devices agree well with the PCE trend of PSCs.

To further observe the carrier recombination and transport mechanism, we examined the electrical impedance spectra (EIS) of the PSCs under dark conditions. EIS measurements were performed at 0 V with a frequency range of 1–1.0 MHz.

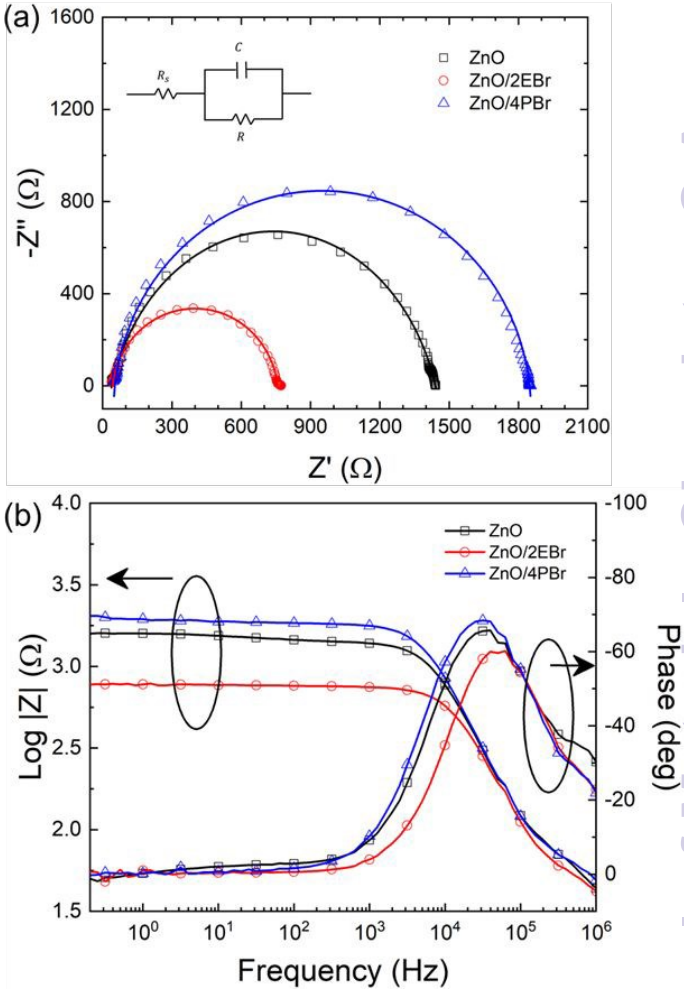

Figure 6. (a) EIS spectra at 0.8 V under dark condition, inset shows the equivalent circuit for analysis of EIS spectra (R_s: Ohmic resistance including the electrodes and bulk resistance, R: resistance associated with the interface charge transport, C: capacitance) and (b) Bode plot.

Figure 6a shows the Nyquist plots of the devices at 0.8 V. The EIS spectra were linearly fitted to estimate the recombination resistance (R_{rec}). A single semi-circle without a transmission line was observed in the Nyquist plots of each devices. Its diameter is assigned as the charge transfer resistance.[53,54] The size of the EIS semi-circle reflects the extent of R_{rec}; thus, depending on the extent of the charge recombination PSCs. The magnitude of the R_{rec} of the devices were 1.51, 0.836, and 1.97 $\mathrm{k\Omega}$ for pristine ZnO, with **2EBr,** and with **4PBr**, respectively. Notably, the device based on ZnO with **4PBr** exhibited the highest R_{rec}, indicating the lowest reduced interfacial recombination. The trend of R_{rec} followed those of the FF and R_{sh} of PSCs. As shown in **Figure 6b**, the peak frequency of the devices followed the trend of the FF and R_{sh}. This indicates that the interlayer also modify the electron life time. Moreover, the electron lifetime (τ) can be estinated using the equatrion $\tau = 1/2\pi f_{mid}$, where f_{mid} is the midfrequency peak of the Bode plot in the impedance spectrum.[53] The estimated τ of the devices based on pristine ZnO, ZnO**/2EBr,** and ZnO**/4PBr** were 25, 13, and 32 μs, respectively. This result supports the EIS analysis results.

Conclusions

Small-molecule electrolytes, **2EBr** and **4PBr**, have been successfully synthesized. The PSC with **2EBr** enhanced PCE, reaching up to 9.56%. PCE was further enhanced by replacing **4PBr** as the interlayer due to the increased ion size and number of ionic functionalities. The enhanced PCE can be mainly attributed to the improvement of J_{sc}. In addition, the trend of the FF followed that of PCEs. The charge-generation, charge-transport, and charge-recombination characteristics also supported the PCE enhancement. As a result, we demonstrated the possibility to maximize performances without complicated synthesis procedures.

Conflicts of interest

There are no conflicts to declare.

Acknowledgements

This research work was supported by the New & Renewable Energy Core Technology Program of the Korea Institute of Energy Technology Evaluation and Planning (KETEP) granted financial resource from the Ministry of Trade, Industry & Energy, Republic of Korea (20193091010110) and was supported by Basic Science Research Program through the National Research Foundation of Korea (NRF) funded by the Ministry of Education (2019R1A2C1002585).

Notes and references

1 G. Yu, J. Gao, J. C. Hummelen, F. Wudl, and A. J. Heeger, *Science,* 1995, **270**, 1789.
2 S. Gunes, H. Neugebauer, and N. S. Sariciftci, *Chem. Rev.*, 2007, **107**, 1324.
3 L. Lu, T. Zheng, Q. Wu, A. M. Schneider, and D. Zhao, L. Yu, *Chem. Rev.*, 2015, **115**, 12666.
4 Y.-W. Su, S.-C. Lan, and K.-H. Wei, *Mater. Today,* 2012, **15**, 554.
5 J. Yuan, Y. Zhang, L. Zhou, H.-L. Yip, T.-K. Lau, X. Lu, C. Zhu, H. Peng, P. A. Johnson, M. Leclerc, Y. Cao, J. Ulanski, Y. Li, and Y. Zou, *Joule*, 2019, **3**, 1140–1151.
6 X. Li, X. Liu, W. Zhang, H.-Q. Wang, and J. Fang, *Chem. Mater.*, 2017, **29**, 4176–4180.
7 Z. Wu, C. Sun, S. Dong, X.-F. Jiang, S. Wu, H. Wu, H.-L. Yip, F. Huang, and Y. Cao, *J. Am. Chem. Soc.*, 2016, **138**, 2004–2013.
8 M. Lv, S. Li, J. J. Jasieniak, J. Hou, J. Zhu, Z. Tans, S. E. Watkins, Y. Li, and X. Chen, *Adv. Mater.*, 2013, **25**, 6889–6894.
9 C. J. Brabec, A. Cravino, D. Meissner, N. S. Sariciftci, T. Fromherz, M. T. Rispens, L. Sanchez, and J. C. Hummelen, *Adv. Funct. Mater.*, 2001, **11**, 374–380.
10 Y. Li, *Acc. Chem. Res.*, 2012, **45**, 723–733.
11 W. Zhang, Y. Wu, Q. Bao, F. Gao, and J. Fang, *Adv. Energy Mater.*, 2014, **4**, 1400359.
12 G. Yu, J. Gao, J. C. Hummelen, F. Wudl, and A. J. Heeger, *Science*, 1995, **270**, 1789–1791.
13 M. H. Hoang, G. E. Park, D. L. Phan, T. T. Ngo, T. V. Nguyen, C. G. Park, M. J. Cho, and D. H. Choi, *Macromol. Res*., 2018, **26**, 844–850.
14 Y. J. Lee, S. J. Jeon, J. Y. Choi, and D. K. Moon, *J. Ind. Eng. Chem.,* 2019, **75**, 138–147.
15 B. Zhu, X. Chen, S. I. Huang, and X. Peng, *Dye. Pigment.*, 2019, **164**, 148–155.
16 S. S. Badge, H. Park, V. H. Tran, and S. H. Lee, *Dye. Pigment*., **2019**, 163, 30–39.
17 S.-H. Oh, S.-I. Na, J. Jo, B. Lim, D. Vak, and D.-Y. Kim, *Adv. Funct. Mater*., 2010, **20**, 1977.
18 S. Nho, G. Baek, S. Park, B. R. Lee, M. J. Cha, D. C. Lim, J. H. Seo, S.-H. Oh, M. H. Song, and S. Cho, *Energy Environ. Sci*., 2016, **9**, 240.
19 Y. Sun, J. H. Seo, C. J. Takacs, J. Seifter, and A. J. Heeger, *Adv. Mater*., 2011, **23**, 1679.
20 C. E. Small, S. Chen, J. Subbiah, C. M. Amb, S.-W. Tsang, T.-H. Lai, J. R. Reynolds, and F. So, *Nat. Photonics,* 2012, **6**, 115.
21 M. Y. Jo, Y. E. Ha, and J. H. Kim, *Sol. Energy Mater. Sol. Cells,* 2012, **107**, 1.
22 M. Y. Jo, Y. E. Ha, and J. H. Kim, *Org. Electron*., 2013, **14**, 995.
23 G. E. Lim, Y. E. Ha, M. Y. Jo, J. Park, Y.-C. Kang, and J. H. Kim, *ACS Appl. Mater. Interfaces,* 2013, **5**, 6508.
24 Y. Li, X. Liu, X. Li, W. Zhang, F. Xing, and J. Fang, *ACS Appl. Mater. Interfaces,* 2017, **9**, 8426.
25 Z. Li, Q. Chen, Y. Liu, L. Ding, K. Zhang, K. Zhu, L. Yuan, B. Dong, Y. Zhou, and B. Song, *Macromol. Rapid Commun.,* 2018, **39**, 1700828
26 Y. H. Kim, N. Sylvianti, M. A. Marsya, J. Park, Y.-C. Kang, D. K. Moon, and J. H. Kim, *ACS Appl. Mater. Interfaces,* 2016, **8**, 32992.
27 Y. H. Kim, N. Sylvianti, M. A. Marsya, D. K. Moon, and J. H. Kim, *Org. Electron.,* 2016, **39**, 163.
28 X. Guo, Y. Zhang, X. Liu, S. Braun, Z. Wang, B. Li, Y. Li, C. Duan, M. Fahlman, J. Tang, J. Fang, and Q. Bao, *Org. Electron.,* 2018, **59**, 15.
29 J. P. Han, E. J. Lee, Y. W. Han, T. H. Lee, and D. K. Moon, *J. Ind. Eng. Chem*., 2016, **36**, 44.
30 M. Gupta, D. Yan, J. Xu, J. Yao, and C. Zhan, *ACS Appl. Mater. Interfaces,* 2018, **10**, 5569.
31 H.-C. Chen, S.-W. Lin, J.-M. Jiang, Y.-W. Su, and K.-H. Wei, *ACS Appl. Mater. Interfaces,* 2015, **7**, 6273.
32 S.-H. Liao, H.-J. Jhuo, Y.-S. Cheng, and S.-A. Chen, *Adv. Mater.,* 2013, **25**, 4766.
33 H. Yang, T. Wu, T. Hu, X. Hu, L. Chen, and Y. Chen, *J. Mater. Chem. C,* 2016, **4**, 8738.
34 X. Li, X. Liu, W. Zhang, H.-Q. Wang, and J. Fang, *Chem. Mater*., 2017, **29**, 4176.
35 Y. H. Kim, D. G. Kim, and J. H. Kim, *Appl. Chem. Eng*., 2016, **27**, 512.
36 T. T. Do, H. S. Hong, Y. E. Ha, J. Park, Y.-C. Kang, and J. H. Kim, *ACS Appl. Mater. Interfaces,* 2015, **7**, 3335.
37 T. T. Do, H. S. Hong, Y. E. Ha, C.–Y. Park, and J. H. Kim, *Macromol. Res*., 2015, **23**, 177.
38 R. Peng, Z. Liu, Q. Guan, L. Hong, W. Song, Q. Wei, P. Gao, J. Huang, X. Fan, M. Wang, and Z. Ge. *J. Mater. Chem. A*, 2018, **6**, 6327–6334.

View Article Online
DOI: 10.1039/D0TC02513E

39 X. Ouyang, R. Peng, L. Ai, X. Zhang, and Z. Ge, *Nat. Photonics*, 2015, **9**, 520–524.
40 Z. Liu, X. Ouyang, R. Peng, Y. Bai, D. Mi, W. Jiang, A. Facchetti, and Z. Ge, *J. Mater. Chem. A*, 2016, **4**, 2530–2536.
41 X. Li, W. Zhang, X. Wang, Y. Wu, F. Cao, and J. Fang, *J. Mater. Chem. A*, 2015, **4**, 504–508.
42 Y. H. Kim, D. G. Kim, R. D. Maduwu, H. C. Jin, D. K. Moon, and J. H. Kim, *Sol. RRL*, 2018, **2**, 1800086.
43 D. G. Kim, Y. H. Kim, R. D. Maduwu, H. C. Jin, D. K. Moon, and J. H. Kim, *J. Ind. Eng. Chem*., 2018, **65**, 175–179.
44 Y. H. Kim, N. Sylvianti, M. A. Marsya, J. Park, Y.-C. Kang, D. K. Moon, and J. H. Kim, *ACS Appl. Mater. Interfaces*, 2016, **8**, 32992−32997.
45 M. Jeong, H. C. Jin, D. K. Moon, and J. H. Kim, *Adv. Mater. Interfaces,* 2019, **6**, 1900797.
46 M. Jeong, H. C. Jin, D. K. Moon, and J. H. Kim, *Dye. Pigment,* 2020, **173**, 107927.
47 B. H. Lee, I. H. Jung, H. Y. Woo, H. K. Shim, G. Kim, and K. K. Lee, *Adv. Funct. Mater*., 24 2041, **24**, 1100–1108.
48 M. Y. Jo, Y. E. Ha, Y. S. Won, S. I. Yoo, and J. H. Kim, *Org. Electron.*, 2015, **25**, 85–91.
49 I. D. Parker, *J. Appl. Phys*., 1994, **75**, 1656.
50 F. Yang, Y. Xu, M. Gu, S. Zhou, Y. Wang, K. Lu, Z. Liu, X. Ling, Z. Zhu, J. Chen, Z. Wu, Y. Zhang, Y. Xue, F. Li, J. Yuan, and W. Ma, *J. Mater. Chem. A*, 2018, **6**, 17688–17697.
51 R. Azmi, S.-H. Oh, and S.-Y. Jang, *ACS Energy Lett.*, 2016, **1**, 100–106.
52 L. J. A. Koster, V. D. Mihailetchi, R. Ramaker, and P. W. M. Blom, *Appl. Phys. Lett.*, 2005, **86**, 123509.
53 H. Kim, H. Jeong, T. K. An, C. E. Park, and K. Yong, *ACS Appl. Mater. Interface*, 2013, **5**, 268–275.
54 H. Wang, G. Liu, X. Li, P. Xiang, Z. Ku, Y. Rong, M. Xu, L. Liu, M. Hu, Y. Yang, and H. Han, *Energy Environ. Sci.,* 2011, **4**, 2025–2029.

View Article Online
DOI: 10.1039/D0TC02513E

Small-molecule electrolytes with diverse ionic functionality as the cathode buffer layer for polymer solar cells

Mijin Jeong[a], Doo Kyung Moon[b], Hyun Sung Kim*[,c], Joo Hyun Kim*[,a]

Table of Contents Entry

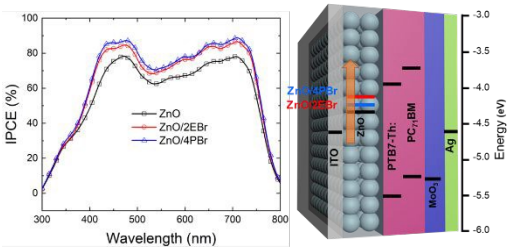

Small-molecule electrolytes were designed and synthesized as the cathode interlayer in inverted polymer solar cells.